Received: 16 May 2022 | Revised: 11 July 2022 | Accepted: 5 August 2022

DOI: 10.1111/ijac.14187

International Journal of Applied Ceramic Technology

RESEARCH ARTICLE

Sol–gel synthesis and characterization of lithium aluminate (L–A–H) and lithium aluminosilicate (L–A–S–H) gels

Sebastian Simon[1] | **Marko Bertmer**[2] | **Gregor J. G. Gluth**[1]

[1]Bundesanstalt für Materialforschung und-prüfung (BAM), Berlin, Germany

[2]Felix Bloch Institute for Solid State Physics, Leipzig University, Leipzig, Germany

Correspondence
Gregor J. G. Gluth, Bundesanstalt für Materialforschung und -prüfung (BAM), Unter den Eichen 87, 12205 Berlin, Germany.
Email: gregor.gluth@bam.de

Funding information
Bundesanstalt für Materialforschung und -prüfung (BAM)

Abstract

Hydrous lithium aluminosilicate (L–A–S–H) and lithium aluminate (L–A–H) gels are candidate precursors for glass-ceramics and ceramics with potential advantages over conventional processing routes. However, their structure before calcination remained largely unknown, despite the importance of precursor structure on the properties of the resulting materials. In the present study, it is demonstrated that L–A–S–H and L–A–H gels with Li/Al ≤ 1 can be produced via an organic steric entrapment route, while higher Li/Al ratios lead to crystallization of gibbsite or nordstrandite. The composition and the structure of the gels was studied by thermogravimetric analysis, X-ray diffraction, ^{27}Al and ^{29}Si magic-angle spinning nuclear magnetic resonance, and Raman spectroscopy. Aluminium was found to be almost exclusively in six-fold coordination in both the L–A–H and the L–A–S–H gels. Silicon in the L–A–S–H gels was mainly in Q^4 sites and to a lesser extent in Q^3 sites (four-fold coordination with no Si–O–Al bonds). The results thus indicate that silica-rich and aluminium-rich domains formed in these gels.

KEYWORDS
aluminosilicates, nuclear magnetic resonance, raman spectroscopy, sol-gel

1 | INTRODUCTION

Glass-ceramics of the Li_2O–Al_2O_3–SiO_2(LAS) system have been extensively studied due to their very low thermal expansion coefficient, excellent thermal shock resistance, high chemical durability, mechanical strength, and specific electrical and optical properties. Because of these properties, they are used in a wide range of applications from the household to space exploration, namely in cook top panels, cookware, stove and furnace windows, gas turbine heat exchangers, satellite and telescope mirror blanks, ring-laser gyroscopes, and electronics packaging,[1,2] and they continue to be researched. Significant research efforts have been devoted to the mobility of Li ions in LAS glasses, making some of these materials fast ion conductors with potential application as solid electrolytes in high energy density batteries.[3,4] Recently, attempts have been reported to produce LAS glass-ceramics or their precursors by additive manufacturing to further widen their range of applicability.[5,6] Related systems without SiO_2, that is, lithium aluminate ceramic materials, too, have beneficial chemical, mechanical, and thermo-physical properties that potentially allow them to be used as a breeder blanket in nuclear fusion reactors and as matrix

in molten carbonate fuel cells,[7–9] and they are also under consideration to be used as ion conductors.[10]

The properties of LAS glasses and glass-ceramics as well as of crystalline lithium aluminates and lithium aluminosilicates depend on their method of synthesis, chemical composition, and thermal history. The traditional process used to produce LAS glass-ceramics involves a two-stage heat treatment of LAS glass. The first stage comprises nucleation in a precursor glass, where $ZrTiO_4$, $Al_2Ti_2O_4$ or ZrO_2 nuclei homogeneously precipitate and allow heterogeneous nucleation of either β-quartz or β-spodumene solid solution; the second stage is the crystallization phase, in which growth of the crystals occurs concomitantly.[1,11–13] However, this high-temperature processing is cost-intensive, and the use of additives can increase the thermal expansion of the resulting materials. This method also requires highly controlled and complex processing to avoid material heterogeneity.

To overcome the disadvantages of the conventional process, alternative methods have been proposed. One method is to produce lithium aluminosilicate ceramics via geopolymerisation or related reactions, that is, the reaction of an aluminosilicate or silicate with an alkaline lithium solution.[6,14,15] However, the most extensively studied method is the sol-gel process, which is generally applicable to the production of glasses, glass-ceramic and ceramics. It combines several advantages, such as high purity, lower sintering temperature, a high degree of homogeneity, small processing time, cost effectiveness, and environment friendliness.[16] This method employs two stages, first the preparation of a gel as precursor, and second the thermal treatment (calcination) of the gel to form the final product, which involves significant structural transformations. Several gel syntheses for preparing LAS glass-ceramics or ceramics have been described in the literature.[17–23] Lithium aluminates as well have been produced from precipitated precursors.[24] It is noted that, strictly, a glass-ceramic is defined as a material whose production involves the controlled crystallization of a parent glass. However, in the context of sol-gel synthesis routes, also the materials with crystalline phases in an amorphous (glassy) matrix, obtained by heat-treatment of the precursor gels, have been called glass-ceramics.[16,18,20] The latter, less restrictive use of the term "glass-ceramics" will be applied in the present study.

Although the properties of glass-ceramics and ceramics are generally affected by the structure of their precursors,[25,26] the precursor gels for LAS glass-ceramic and ceramics production have been studied only to a very limited extent. Some studies relating to the production of LAS glass-ceramics via the sol-gel process report only X-ray diffraction (XRD) and thermal analysis data of the precursor gels before calcination, which mainly serve to demonstrate that the gel is amorphous and transforms to crystalline phases on heating but do not allow conclusions to be drawn as regards the atomic-scale structure of the gels.[18,22] In cases when spectroscopic data are presented, they are usually limited to Fourier-transform infra-red spectra,[19,23] for which interpretation can be ambiguous.[21–23] Thus, little is known as regards the structure of gels in the Li_2O–Al_2O_3–SiO_2(–H_2O) system, in marked contrast to a number of other silicate gels with comparable technological importance.

To gain insight into the local structure of these gels, stoichiometrically controlled, amorphous Li_2O–Al_2O_3–H_2O (L–A–H), Li_2O–Al_2O_3–SiO_2–H_2O (L–A–S–H) and Al_2O_3–SiO_2–H_2O (A–S–H) gels were synthesized in the present study, and the gels were characterized by XRD, thermogravimetric analysis (TGA), ^{27}Al and ^{29}Si magic-angle spinning nuclear magnetic resonance (MAS NMR) spectroscopy, and Raman spectroscopy. Characterization of the gels was performed with no previous calcination (only drying was conducted) to obtain data relating to the initial structure of the gels. A reliable synthesis route was successfully developed, and the spectroscopic data enabled a more detailed structural description of the resulting gels than was hitherto available. In addition, selected L–A–S–H gels were heated to 1000°C, and the resulting LAS materials were analyzed by XRD.

2 | MATERIALS AND METHODS

2.1 | Synthesis of the gels

Starting materials for the syntheses of the gels were aluminium nitrate nonahydrate [$Al(NO_3)_3{\cdot}9H_2O$; Honeywell Fluka, Muskegon, MI, USA], lithium nitrate ($LiNO_3$; Merck, Darmstadt, Germany) and colloidal silica (50 wt% SiO_2 in water; Ludox TM-50 colloidal silica; Sigma Aldrich, St. Louis, MO, USA). The pureness and crystallinity of the starting materials was inspected by XRD and Raman spectroscopy (Supplementary Material available online, Figures S1 and S2).

L–A–H, L–A–S–H, and A–S–H gels with the nominal molar ratios listed in Table 1 were synthesized using the organic steric entrapment route[27] as modified by Walkley et al.[28] with additional adjustments required to produce gels of the specified compositions as follows (see also Figure S3): A 5 wt% polyethylene glycol (PEG) solution was produced by adding small increments of PEG (Sigma Aldrich, St. Louis, MO, USA; number average molecular weight $M_n \approx 20{,}000$ Da) to ultrapure water, and the resultant solution was stirred at 60°C for 1 h. $Al(NO_3)_3{\cdot}9H_2O$ and $LiNO_3$ were added to distilled water to produce 40 wt% solutions of anhydrous salts with the specified Li/Al ratio

TABLE 1 Designations, chemical formula, atomic ratios, and crystalline analogues of the A–S–H, L–A–H, and L–A–S–H gels

Designation	Formula (unhydrous)	Li/Al	Si/Al	Crystalline analogue
A-S-H 6:2	$Al_6Si_2O_{13}$	–	0.33	Mullite
L-A-H 1:11	$LiAl_{11}O_{17}$	0.09	–	Lithium undecaaluminate
L-A-H 1:5	$LiAl_5O_8$	0.20	–	Lithium pentaaluminate
L-A-H 1:1	$LiAlO_2$	1.00	–	Lithium aluminate
L-A-H 5:1	Li_5AlO_4	5.00	–	–
L-A-S-H 1:1:1	$LiAlSiO_4$	1.00	1.00	Eucryptite
L-A-S-H 1:1:1.85	$LiAlSi_{1.85}O_{5.7}$	1.00	1.85	–
L-A-S-H 1:1:2	$LiAlSi_2O_6$	1.00	2.00	Spodumene
L-A-S-H 1:1:3	$LiAlSi_3O_8$	1.00	3.00	Li-orthoclase
L-A-S-H 1:1:4	$LiAlSi_4O_{10}$	1.00	4.00	Petalite
L-A-S-H 1:2:2	$LiAl_2Si_2O_{7.5}$	0.50	1.00	–
L-A-S-H 1:2:4	$LiAl_2Si_4O_{11.5}$	0.50	2.00	–
L-A-S-H 1:2:6	$LiAl_2Si_6O_{15.5}$	0.50	3.00	–
L-A-S-H 1:2:8	$LiAl_2Si_8O_{19.5}$	0.50	4.00	–

(only $Al(NO_3)_3$ for the A–S–H gel). This solution was subsequently added to the 5 wt% PEG solution and the resulting mixture stirred at 60°C for 1 h. For the L–A–S–H gels and the A–S–H gel, colloidal silica was subsequently added to the mixture to yield the specified Al/Si ratio and the solution stirred again at 60°C for 1 h. Water was evaporated from the resulting solution by stirring at 80°C to form a viscous gel, which was then placed in an oven at 100°C overnight to remove excess water and nitrate. Since the gels were not calcined at higher temperatures, PEG and nitrate impurities remained in the materials, as will be discussed in Sections 3.2 and 3.5. Finally, the solid gel was manually ground to a powder and homogenized.

The compositions of most gels were specified to correspond to crystalline compounds occurring in ceramic processing and/or as natural minerals. In addition, a L–A–H gel with "excess" Li (Li/Al = 5), L–A–S–H gels with Li/Al = 0.5, and a L–A–S–H gel with a composition (Li/Al = 1, Si/Al = 1.85) corresponding to the mix employed in a previous study on additive manufacturing of LAS materials[6] were produced and analyzed. The sample designations in Table 1 reflect the numbers of Li, Al, and Si per unit formula; water contents are not considered in the designations, as these are variable and depend on the drying history.

Figure 1 shows the compositions of the gels plotted onto the Li_2O–Al_2O_3–SiO_2 ternary diagram; this projection ignores the variable and a priori unknown water content of the gels as well as any auxiliary agents and depicts only their relative fractions of Li_2O, Al_2O_3, and SiO_2. Thus, a material produced from a specific gel by calcination until complete dehydration and loss of auxiliary agents would have the chemical composition shown in the diagram for that gel. The L–A–S–H gels lie in the compositional range of potential glass formation,[29] making them potential precursors for LAS glasses and glass-ceramics.

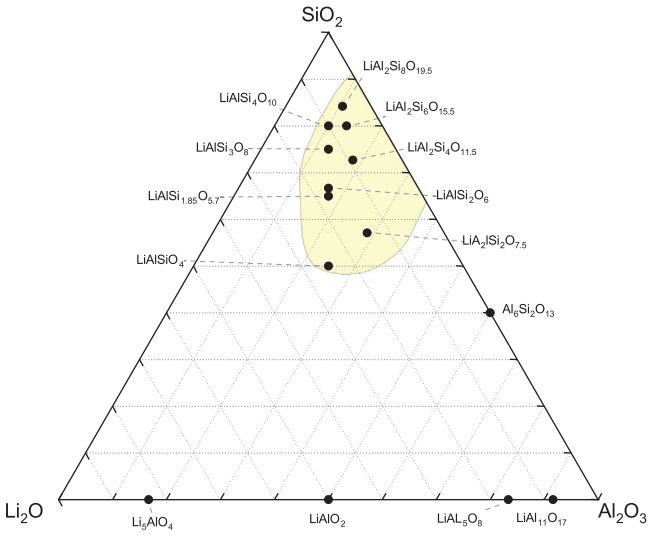

FIGURE 1 Gel compositions plotted onto the Li_2O–Al_2O_3–SiO_2 ternary diagram. The approximate compositional range of potential glass formation[29] is marked yellow.

2.2 | XRD

To collect XRD patterns, a laboratory X-ray diffractometer (Ultima IV, Rigaku, Tokyo, Japan) was used in

Bragg-Brentano geometry with Cu Kα radiation (40 kV, 40 mA) and a Si strip detector (D/teX Ultra) with 5° Soller slits. To reduce the background from the sample holder, a Si single crystal cut at (911) orientation was employed as the sample holder. A divergence slit of 0.5° (10 mm axial) was used; the beam knife was installed to minimize low-angle air scattering. All diffractograms were recorded in the range 5–65° 2θ, with a step width of 0.02° at a scan speed of 0.5° 2θ/min. To evaluate the diffraction data, the Match! programme in combination with the powder diffraction file PDF-2 (2003) database was used.

2.3 | TGA

For TGA (TGA device STA 449C, Netzsch, Selb, Germany), the sample material was heated from 35°C to 1000°C, with a heating rate of 10°C/min under a nitrogen flow of 80 ml/min. For each measurement, ~35 mg of the sample material was filled in an Al_2O_3 crucible and placed in the TGA system. To remove oxygen and, thus, prevent oxidation during the measurements, the furnace was first evacuated and subsequently filled with nitrogen before the measurements. From the recorded TGA curves, their derivatives (differential thermogravimetric [DTG] curves) were computed.

Samples of selected L–A–S–H gels were retrieved from the TGA device after heating to 1000°C and subsequently analyzed by XRD (see Section 2.2 for measurement conditions) to determine the phase assemblage of the resulting LAS materials.

2.4 | MAS NMR spectroscopy

^{27}Al MAS NMR experiments (spectrometer AVANCE 750, Bruker, Billerica, USA) were carried out at a magnetic field strength of 17.6 T and a frequency of 195.06 MHz. A spinning frequency of 12 kHz and a 4 mm probe were used. The pulse length was 1 µs, corresponding to a pulse angle of less than 30°. At least 1000 scans were accumulated per specimen, and the recycle delay was set to 0.1 s. ^{27}Al chemical shifts were referenced to a 1 M solution of aluminium nitrate by using K-alum as a secondary reference at 0.7 ppm.[30]

^{29}Si MAS NMR spectra were collected on the same spectrometer at a frequency of 148.68 MHz. The spectra were acquired with a single 90° pulse with a pulse length of 2.5 µs and a recycle delay of 10 s. Typically, about 6000 scans were accumulated per specimen. ^{29}Si chemical shifts were referenced to tetramethylsilane (TMS).

The NMR spectra were processed and the resonances fitted with the Dmfit programme.[31]

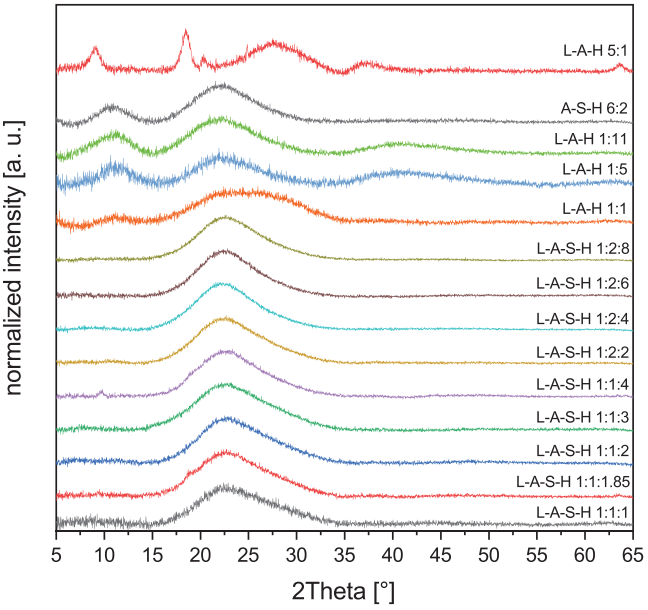

FIGURE 2 Background-corrected and normalized X-ray diffraction (XRD) patterns (Cu Kα radiation) of the gels

2.5 | Raman spectroscopy

Raman spectra were collected at room temperature using a confocal WITec Alpha300R instrument with a laser wavelength of 532 nm and a laser power of 4 mW. A ×100 objective was employed, resulting in a diameter of the incident focused laser beam of ~1 µm. The spectrometer grating had 600 lines/mm, yielding a spectral resolution of ~4.5 cm^{-1}. For each sample, 25 spectra in the range 200–4000 cm^{-1} were recorded, each with an acquisition time of 2 s, and averaged to improve the signal-to-noise ratio. Background correction and normalization of the Raman spectra was carried out with the Witec Project Four80/160 programme.

3 | RESULTS

3.1 | XRD

The XRD patterns of the gels are shown in Figure 2 (the XRD patterns with the *d*-spacing plotted on the abscissa are shown in Figure S4). Except for L-A-H 5:1 and L-A-S-H 1:1:4, the gels were X-ray amorphous. The weak reflection at ~9.7° 2θ in the diffractogram of L-A-S-H 1:1:4 is attributed to a minor unknown impurity in that gel.

The diffractogram of L-A-H 5:1 is dominated by a broad hump around 27.5° 2θ (maximum at $d \approx 3.2$ Å) and peaks at 8.85, 18.36, 20.36, 24.80, and 63.50° 2θ. The reflections at 18.36 and 20.36° 2θ as well as a minor hump around 37° 2θ are attributed to gibbsite or nordstrandite [both $Al(OH)_3$].

The assignment of the other peaks is uncertain; nevertheless, they demonstrate that synthesis of a fully amorphous gel with the composition L-A-H 5:1 (Li/Al = 5) was not possible under the present experimental conditions. It is noted that the peaks with uncertain assignment could not be matched with the patterns of zabuyelite (Li_2CO_3) or the carbonate-bearing Li–Al layered double hydroxide (LDH) $Li_2Al_4(OH)_{12}(CO_3)\cdot 3H_2O$.

The other L–A–H gels were fully amorphous, according to their XRD patterns. The patterns of L-A-H 1:11 and L-A-H 1:5 exhibit broad humps around ~11, 22, and 41° 2θ (maxima at $d \approx 8.2$, 4.0, and 2.2 Å, respectively). Similarly, the pattern of A-S-H 6:2, whose composition is dominated by Al as well, exhibits humps around ~11 and 22° 2θ ($d \approx 8.2$ and 4.0 Å, respectively), indicating that the structure of the Al-rich gels bears some similarities. In the diffractogram of L-A-H 1:1, in which the number of Al atoms is balanced by Li, humps are present at ~11° 2θ (maximum at $d \approx 8.2$ Å) and in the range ~17–34° 2θ (d in the range 2.5–5 Å), signifying that its structure differed from the more Al-rich gels.

The diffractograms of the L–A–S–H gels differ significantly from XRD patterns of the L–A–H gels and A–S–H gel, indicating different local structures. Namely, the diffractograms exhibit a broad asymmetric peak in the range ~15–35° 2θ (maximum at $d \approx 4.0$ Å), which is slightly shifted to lower diffraction angles with increasing Si content, demonstrating subtle structural changes with varying composition.

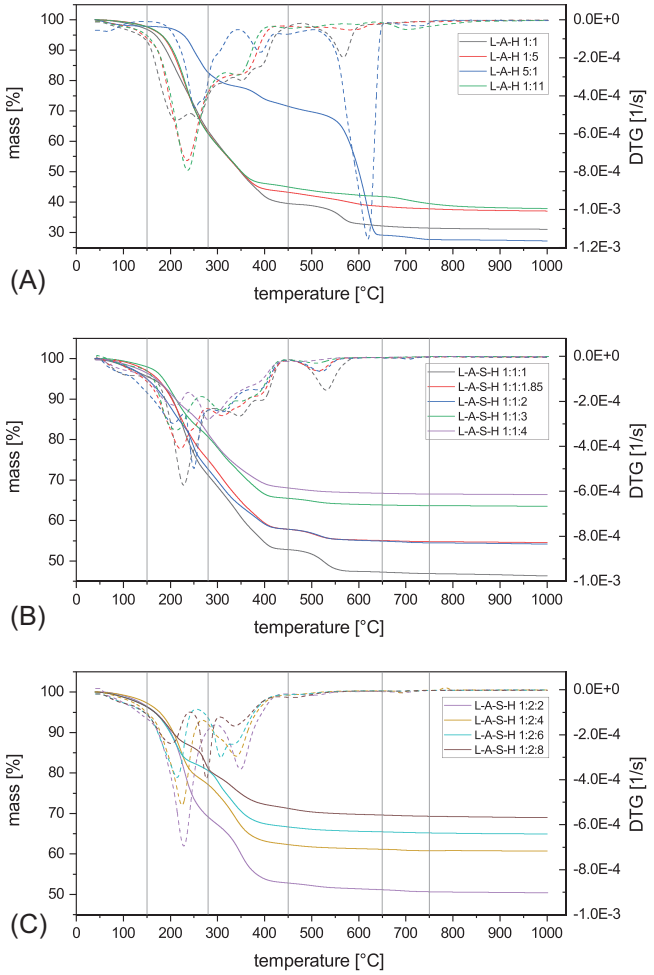

FIGURE 3 Thermogravimetric analysis (TGA) and differential thermogravimetric (DTG) curves of the L–A–H gels (A) and the L–A–S–H gels (B and C). The vertical grey lines indicate temperatures of 150, 280, 450, 650 and 750°C, respectively

3.2 | TGA

Figure 3 shows the TGA curves and the DTG curves of the L–A–S–H and L–A–H gels in the range 40–1000°C, obtained with a heating rate of 10°C/min in nitrogen. Based on comparison with published TGA/DTG curves of nitrate-bearing Li–Al LDH[32] and Ca–Al LDH,[33] and aluminosilicate gels whose production involved PEG[28] and/or nitrates,[21,22] the observed mass losses are assigned as follows: Dehydration (i.e., loss of molecular water) occurred in the range 40–150°C; the two TGA steps in the ranges 150–280°C and 280–450°C, respectively, are attributed to dehydroxylation (i.e., condensation of hydroxyl groups and loss of water), decomposition of PEG, and reduction of remaining amounts of nitrate (NO_3^-) to yield nitrite (NO_2^-); the mass losses at ~450–650°C and ~650–750°C are attributed to the decomposition of nitrite and resumed dehydroxylation. The TGA step at 450–650°C could, in principle, be also assigned to release of CO_2 from $Li_2Al_4(OH)_{12}(CO_3)\cdot 3H_2O$[34]; however, the XRD results show that this phase was not present in the gels.

For L-A-H 5:1, the TGA step at ~600°C was very prominent, indicating that this gel retained the largest amount of nitrate after drying. The decomposition of gibbsite, which was found by XRD in L-A-H 5:1, contributed to the mass loss in the range ~200–350°C of that gel. The TGA curves of the other L–A–H gels were broadly similar to each other, with the total mass loss slightly increasing with increasing Li/Al ratio. In these gels, most of the mass loss occurred in the range 150–450°C, indicating that high amounts of PEG had remained in the gels after drying.

The total mass losses of the L–A–S–H gels were generally lower than those of the L–A–H gels, while the general characteristics of their TGA/DTG curves resembled those of the L–A–H gels with low Li/Al ratios. Again, the highest TGA steps are found in the range 150–450°C, attributed to remaining PEG and hydroxyl groups in the gels.

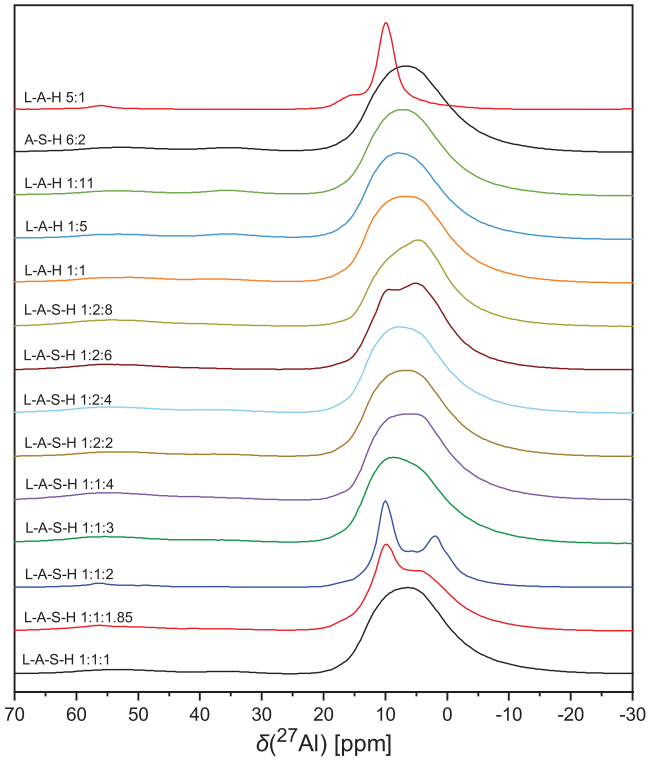

FIGURE 4 ^{27}Al magic-angle spinning nuclear magnetic resonance (MAS NMR) spectra of the gels. The weak broad signal around 55 ppm is a spinning sideband.

3.3 | ^{27}Al MAS NMR spectroscopy

^{27}Al MAS NMR spectra of the gels are shown in Figure 4. The spectra of all gels are dominated by a resonance, or in some cases two resonances, in the range from 20 to −10 ppm, that is, in the chemical shift range of 6-coordinated aluminium (AlO_6). In addition, the spectra of most gels exhibited a considerably smaller, broad signal around 32 ppm, indicating the presence of minor amounts of 5-coordinated aluminium (AlO_5). The small, broad signal around 55 ppm is a spinning sideband; it cannot be excluded that there is also a minor resonance of 4-coordinated aluminium (AlO_4) in this range, but if present its amount would have been very low.

To determine the fractions of the different Al species, the resonances were fitted using the Czjzek model for a quadrupolar line with a distribution of the isotropic chemical shifts[35] for the broad, usually dominating signal in the AlO_6-range; a Gaussian function for the second, narrower resonance in that range, if such a signal was identified; and a Gaussian function for the signal of AlO_5 around 32 ppm. The resulting isotropic chemical shifts and site abundances are listed in Table S1.

The very broad resonance (fitted with the Czjzek model) in the range 20 ppm to −10 ppm of the ^{27}Al MAS NMR spectra of all gels indicates a wide distribution of Al-O distances and bond angles, that is, AlO_6 in an amorphous phase or phases. This was usually the dominant species, and its chemical shift (Czjzek model) was mostly centred in the range 8.0−12.5 ppm. However, for L-A-S-H 1:1:1.85 and L-A-S-H 1:1:2, in which high amounts of AlO_6 in a more ordered environment were found (see below), fitting of the AlO_6 in the amorphous phase yielded chemical shifts of 3.8 and 2.6 ppm, respectively. For L-A-H 5:1, the maximum of the broad resonance that was present in addition to that of the gibbsite (see below) was found at 17.9 ppm.

The spectrum of L-A-H 5:1 is dominated by a comparatively narrow signal at ~10 ppm. This signal required fitting with two resonances, one at 9.9 ppm and a smaller one at 8.4 ppm. These are attributed to AlO_6 in gibbsite,[36] identified in this gel also by XRD; the fraction (i.e., the molar fraction, referred to all Al species in the material combined) of these AlO_6 species in L-A-H 5:1 was determined to be 53.9 %. Similarly, the spectra of L-A-S-H 1:1:1.85, L-A-S-H 1:1:2, L-A-S-H 1:1:4, and L-A-S-H 1:2:6 exhibited a comparatively narrow resonance in the chemical shift range 10.0−11.3 ppm. However, in none of these gels were crystalline compounds detected by XRD (except a minor impurity in L-A-S-H 1:1:4), demonstrating that the domain sizes of the phases containing the pertinent AlO_6 species were generally too small to give diagnostic reflections in the XRD patterns. It is noted that the highest fractions of this AlO_6 species were determined for L-A-S-H 1:1:1.85 (37.6 %) and L-A-S-H 1:1:2 (54.5 %), that is, the L–A–S–H gels with a Si/Al = 1.85 and Si/Al = 2, respectively.

The fractions of AlO_5 in the gels ranged from ~0% to 4.1 %, with a trend of higher amounts in the L–A–H gels and the A–S–H gel (2.3−4.1 %; L-A-H 5:1 excluded), compared to the L–A–S–H gels (~0−2.6%). L-A-H 5:1 contained virtually no AlO_5.

3.4 | ^{29}Si MAS NMR spectroscopy

For six of the nine L–A–S–H gels, ^{29}Si MAS NMR spectra were acquired; these are shown in Figure 5. All spectra exhibit a major broad resonance in the range −105 ppm to −120 ppm, and a considerably smaller, broad resonance centred at approximately −102 ppm. The larger peak can be unequivocally assigned to Q^4 species (fully polymerized SiO_4 tetrahedra), while the smaller resonance may, in principle, be attributed to Q^3 species (i.e., SiO_4 tetrahedra connected to three other SiO_4 tetrahedra via bridging oxygens and to one OH group) as well as to $Q^n(m\text{Al})$ species with $m \geq 1$ (i.e., SiO_4 tetrahedra which are connected to at least one AlO_4 tetrahedron via bridging oxygen). According to the ^{27}Al MAS NMR spectra, however, AlO_4

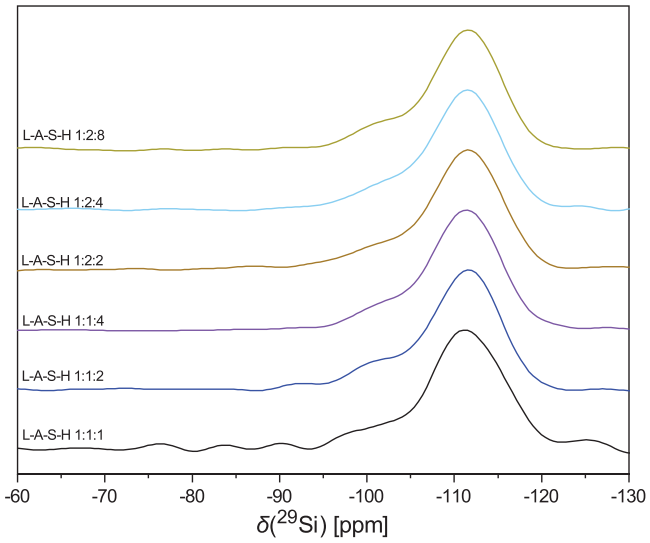

FIGURE 5 ^{29}Si magic-angle spinning nuclear magnetic resonance (MAS NMR) spectra of the L–A–S–H gels

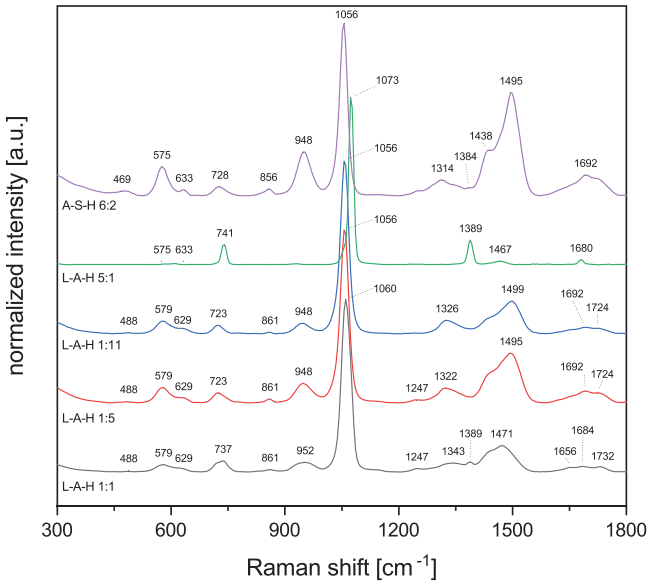

FIGURE 6 Background-corrected and normalized Raman spectra of the L–A–H gels and the A–S–H gel in the range 300–1800 cm^{-1}

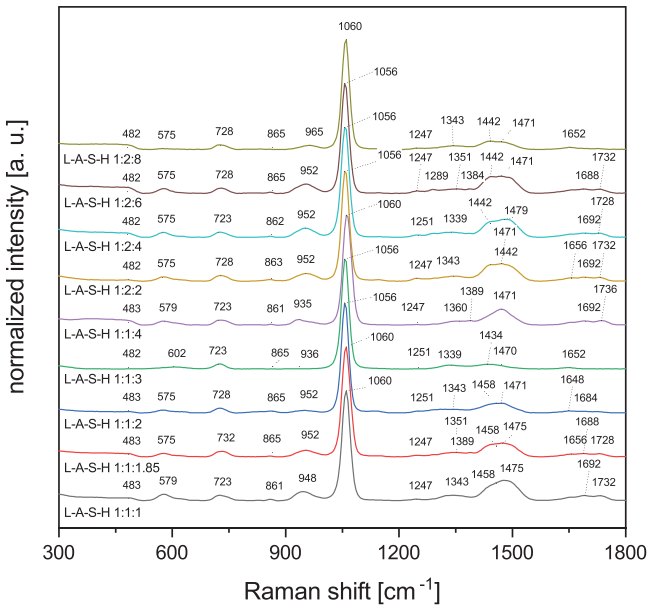

FIGURE 7 Background-corrected and normalized Raman spectra of the L–A–S–H gels in the range 300–1800 cm^{-1}

tetrahedra were not present or present only in very small amounts in the L–A–S–H gels (Section 3.3); thus, no or only very minor amounts of $Q^n(m\text{Al})$ sites could exist in the gels. It is therefore concluded that the resonance around −102 ppm represents Q^3 species that were present in addition to the more abundant Q^4 species. In the spectra of L-A-S-H 1:1:2, L-A-S-H 1:2:2, and L-A-S-H 1:2:4, minor signals centred at approximately −95 ppm may be discerned in addition to the two resonances just discussed. Following the same line of argument, these minor signals can be assigned to minor amounts of Q^2 species (i.e., SiO_4 tetrahedra connected to two other SiO_4 tetrahedra via bridging oxygens) in the gels.

Fitting of the resonances, using Gaussian functions, yielded ~85 % Q^4 species, ~15 % Q^3 species, and ≤6 % Q^2 species in the gels (Table S2). These numbers are in line with silica gel-like domains in the L–A–S–H gels, with the Q^4 sites located mainly in the core and Q^3 and fewer Q^2 species in the outer layer of the domains.

3.5 | Raman spectroscopy

Raman spectra of the gels were acquired with a laser wavelength of 532 nm and a laser power of 4 mW at room temperature; the background-corrected and normalized spectra in the range 300–1800 cm^{-1} are shown in Figures 6 and 7. The spectra of all gels exhibit two prominent bands at ~1440 and 1470–1500 cm^{-1} as well as less intense signals at ~860, 1250, 1290, 1314, 1655, 1690 and 1730 cm^{-1}, caused by the PEG in the materials.[37,38] The other bands can be partly assigned to structural units of the inorganic phases constituting the gels. A list of potentially relevant structural units in various amorphous, semi-crystalline and crystalline silicates, aluminosilicates and aluminates, with the energy ranges of the associated bands in their Raman spectra, is provided in Table S3; a summary of the assignments for the present gels is provided in Table 2 and will be discussed in more detail below.

For the L–A–H gels, the most prominent band in their Raman spectra is the peak at ~1060 cm^{-1}, assigned to the nitrate groups[33,39] that had remained in the gels after

TABLE 2 Assignments of the bands in the Raman spectra of the L–A–H, A–S–H, and L–A–S–H gels

Spectral range (cm^{-1})	Structural unit/compound	Vibration	L–A–H	A–S–H	L–A–S–H	References
469–488	SiO_2/Q^4; AlO_4^{5-}	Si–O symmetric stretching; Al–O stretching	(X)[a]	X (X)[a]	X (X)[a]	43; 41
575–602	AlO_6^{9-}; $Si_2O_5^{2-}/Q^3$	Al–O stretching; Si–O–Si motion (incl. bending)	X	X X	X X	33,40–42; 43–45
629–633	AlOH	O–H bending	X	X	X	40
723–741	NO_3^-	N–O degenerate symmetric stretching/planar angular deformation	X	X	X	33,39
~860	PEG		X	X	X	37
935–965	AlOH	O–H bending	X	X	X	40
1056–1073	NO_3^-; $Si_2O_5^{2-}/Q^3$	N–O symmetric stretching; Si–O symmetric stretching	X	X X	X X	33,39; 43–46
~1250	PEG		X	X	X	37,38
~1290	PEG		X	?	X	37,38
~1314	PEG		X	X	X	38
1330–1389	NO_3^-	N–O asymmetric stretching	X	X	X	39
~1440	PEG		X	X	X	37,38
1470–1500	PEG		X	X	X	37,38
~1655	PEG		X	X	X	38
~1690	PEG		X	X	X	38
~1730	PEG		X	X	X	38

[a]No or only minor amounts of AlO_4 units were present in the gels, according to the ^{27}Al MAS NMR spectra.

drying. In the spectrum L-A-H 5:1, this band is slightly shifted to 1073 cm^{-1}, indicating a different chemical environment of that group, compared to the other L–A–H gels, which may be explained by its different composition (Li/Al = 5). Furthermore, in the spectrum of this gel, the intensity of the nitrate bands at 741, 1073, and 1389 cm^{-1}[33,39] are strongly enhanced, compared to the other gels, in line with the TGA results, which demonstrate that the highest amount of nitrate was present in L-A-H 5:1.

In the Raman spectra of the other L–A–H gels and the A–S–H gel, the bands at ~730, 1060, and 1330 cm^{-1} reveal the presence of remaining nitrate groups as well, but at a lower amount than in L-A-H 5:1. The bands at ~950 and ~630 cm^{-1} cannot be unequivocally assigned, but it is likely that these are related to OH bending vibrations, comparable to the vibrations observed in the different polymorphs of AlO(OH) and $Al(OH)_3$.[40] The comparatively strong band found at 575 or 579 cm^{-1} in the spectra of the L–A–H gels and the A–S–H gel is assigned to the Al–O symmetric stretching of their AlO_6 units.[33,40–42] A weak band at 469 cm^{-1} in the spectrum of A-S-H 6:2 is likely related to the Si–O–Si symmetric stretching vibrations of Q^4 species.[43] The very weak band at 488 cm^{-1} in the spectra of the L–A–H gels is not related to Si species; it cannot be unequivocally assigned but, since the ^{27}Al MAS NMR spectra do not completetly rule out the presence of minor amounts of AlO_4 units, it is possibly related to Al–O stretching vibrations of such species.[41]

The Raman spectra of all L–A–S–H gels are similar to each other and have in common a strong peak at ~1060 cm^{-1}. This band is caused, at least partly, by nitrate groups[33,39] that had remained in the materials. This is again demonstrated by the occurrence of two smaller bands at ~730 and 1340–1360 cm^{-1}, respectively, also characteristic of the nitrate group.[33,39] However, the strong peak at ~1060 cm^{-1} is also in the Raman shift region of Si–O symmetric stretching vibrations of Q^3 species,[43–46] in line with the presence of this species in the L–A–S–H gels, and likely also in the A–S–H gel. As discussed in Section 3.4, the presence of $Q^n(m\text{Al})$ species with $m \geq 1$ that would cause bands in the same region can be ignored for the interpretation of the Raman spectra of the L–A–S–H gels, since AlO_4 is not present or present at a very minor amount in the gels. The comparatively strong band observed at ~950 cm^{-1} is attributed to OH

bending vibrations as above. The band found at, or close to, 575 cm^{-1} in the spectra of the L–A–S–H gels is assigned to the Al–O symmetric stretching of the AlO_6 units,[33,40–42] as for the L–A–H gels and the A–S–H gel. It is plausible, however, that also Si–O–Si bending vibrations of the Q^3 species[43–45] in the L–A–S–H gels contributed to this band. The generally weak signal at ~482 cm^{-1} is assigned to Si–O–Si symmetric stretching vibrations of the Q^4 species[43] in the gels, and possibly also to Al–O stretching vibrations of minor amount of AlO_4 units,[41] if these were present at all.

The Raman spectra in the hydroxyl and water stretching region (Figures S5 and S6) of all gels except L-A-H 5:1 exhibit a broad, featureless band in the range ~3300−3620 cm^{-1}, that is, narrow peaks of specific hydroxyl groups cannot be identified in the spectra. This is consistent with a wide distribution of water and hydroxyl species and their environments, in accord with the amorphous nature of the gels as demonstrated by the XRD results. The broad band in that region of the normalized spectrum of L-A-H 5:1 (Figure S5) is much less prominent, compared to the other gels, at least partly due to the fact that this spectrum is dominated by the very strong nitrate peaks.

3.6 | XRD of heat-treated L–A–S–H gels

The XRD patterns of the L–A–S–H gels after heating to 1000°C in the TGA device are shown in Figure 8. The samples had cooled down to room temperature naturally, that is, a controlled cooling or quenching regime was not applied. Nevertheless, the materials resulting from heating L-A-S-H 1:2:6 and L-A-S-H 1:2:4 (hereafter denoted LAS 1:2:6 and LAS 1:2:4, respectively) contained a significant fraction of amorphous phase, evidenced by a broad hump in their XRD patterns around 22.5° 2θ ($d \approx 4.0$ Å). In the diffractogram of LAS 1:2:6, minor peaks are present at 23.1, 26.1, and 49.0° 2θ, likely related to the presence of β-spodumene-type lithium aluminosilicate ($LiAlSi_{3.75}O_{9.5}$; PDF # 00-053-1278)[47] or mullite (Al_4SiO_8; PDF # 01-084-1205). LAS 1:2:4 contained more significant fractions of crystalline phases, viz. β-quartz (SiO_2; PDF # 01-089-8950), $LiAlSi_{3.75}O_{9.5}$ with a β-spodumene-type structure (PDF # 00-053-1278),[47] $LiAlSi_2O_6$ with a β-quartz-type structure (PDF # 00-031-0706),[48] and alumina (Al_2O_3; PDF # 01-080-0955). The position of the amorphous humps in both materials was close to the position of the hump in their respective precursor gels (Figure 2). However, heating to 1000°C had removed virtually all water and auxiliary agents from the materials (see the TGA/DTG curves, Figure 3), meaning that the LAS materials were water-free and had undergone significant structural transformations.

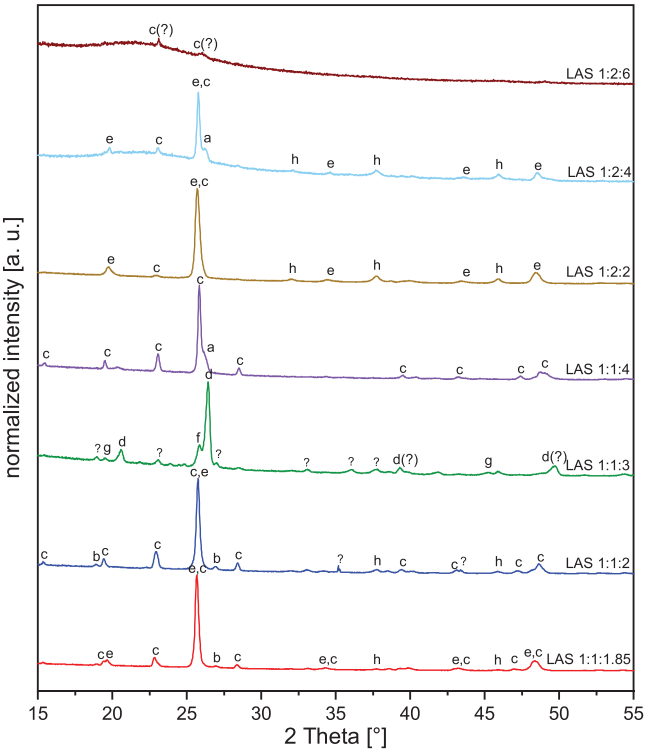

FIGURE 8 X-ray diffraction (XRD) patterns (Cu Kα radiation) of L–A–S–H gels after heating to 1000°C. Major reflections are labeled a, SiO_2 (β-quartz); b, Li_2SiO_3; c, $LiAlSi_{3.75}O_{9.5}$ (β-spodumene-type structure); d, $LiAlSi_{3.5}O_9$ (virgilite: β-quartz-type structure); e, $LiAlSi_2O_6$ (β-quartz-type structure); f, $LiAlSiO_4$ (β-eucryptite); g, α-$LiAlO_2$; h, Al_2O_3

The LAS materials obtained by heating L-A-S-H 1:1:1.85, L-A-S-H 1:1:2, L-A-S-H 1:1:3, L-A-S-H 1:1:4, and L-A-S-H 1:2:2 (hereafter denoted LAS *x*:*y*:*z* according to the respective Li:Al:Si ratios of the precursor gel) did not contain a high amount of amorphous phase. The crystalline phases observed in these materials were β-quartz (SiO_2; PDF # 01-089-8950), lithium metasilicate (Li_2SiO_3; PDF # 01-072-1140), $LiAlSi_{3.75}O_{9.5}$ with a β-spodumene-type structure (PDF # 00-053-1278),[47] virgilite with a β-quartz-type structure (approximately $LiAlSi_{3.5}O_9$; PDF # 01-031-0707),[49] $LiAlSi_2O_6$ with a β-quartz-type structure (PDF # 00-031-0706),[48] β-eucryptite ($LiAlSiO_4$; PDF # 01-073-0255), α-$LiAlO_2$(PDF # 01-074-2232), and alumina (Al_2O_3; PDF # 01-080-0955), depending on the composition of the precursor gel (Figure 8). The stoichiometric β-eucryptite ($LiAlSiO_4$) and α-$LiAlO_2$ were only observed in LAS 1:1:3; the diffractogram of this material also contained reflections of virgilite, and additional peaks that could not be unequivocally assigned. The diffractogram of LAS 1:1:2 contained additional peaks of unidentified crystalline phase(s) at 35.2 and 43.4° 2θ.

4 | DISCUSSION AND CONCLUSIONS

The present results demonstrate that the organic steric entrapment method[27,28] can be applied to synthesize L–A–H and L–A–S–H gels, which are candidate precursors for the production of glass-ceramics and ceramics, if the Li/Al ratio of the starting solution is below a certain limit (Li/Al ≤ 1.0 in the current study).

The L–A–H gels with Li/Al ≤ 1.0 were fully amorphous to X-rays (Cu Kα radiation). Aluminium in these gels was almost exclusively in six-fold coordination (AlO_6), demonstrating structural similarities with gibbsite [$Al(OH)_3$]. In addition, low amounts of AlO_5 were identified in the gels by ^{27}Al MAS NMR; possibly a very minor amount of AlO_4 was present as well. These results are in line with previous work,[50] which identified AlO_6, AlO_5, and AlO_4 units in hydrous amorphous alumina precipitated from $AlCl_3$/NaOH solutions. It may be anticipated that the Li in the L–A–H gels occupies octahedral sites, thus creating local structures that resemble the structure of Li–Al LDHs.[32,34,51] Alternatively, Li may be intercalated between $Al(OH)_3$ layers in the gels.[52] No attempt was made in the present study to differentiate between these possibilities; thus, this issue needs to be evaluated in future work.

The L–A–S–H gels as well were generally X-ray amorphous (except a minor impurity in L-A-S-H 1:1:4). XRD indicated that aspects of their local structure differed from that of the L–A–H gels, in line with their different chemical compositions. However, as for the latter, Al in the L–A–S–H gels was almost exclusively in six-fold coordination. Si was mostly (~85 %) in Q^4 sites, with the remainder mainly in Q^3 sites, both essentially not associated with Al. This distribution of Si species indicates that Si-rich domains had formed in the gels, with Q^4 species in the core and Q^3 species mainly located in the outer layer of the domains. Taken together, the present results suggest that Al and Si are not homogeneously distributed in the L–A–S–H gels but instead form separate alumina gel-like and silica gel-like domains during precipitation. As for the L–A–H gels, the structural role of Li in the L–A–S–H gels as well as its distribution between the domains of the gels remains to be clarified in future studies.

After synthesis and drying at 100°C, as applied in the present study, the gels contained considerable amounts of PEG, water, and nitrate, which were applied in the synthesis. TGA showed that dehydration and loss of PEG and nitrate/nitrite is completed at ~800°C for the L–A–H gels, while the L–A–S–H gels were completely dehydrated and the auxiliary agents lost already at ~600°C. Heating the L–A–S–H gels to 1000°C led to the formation of crystalline lithium aluminosilicates and silicates when Li/Al ratio of the gel was 1, while the same treatment of some of the L–A–S–H gels with Li/Al = 0.5 led to the formation of a mostly amorphous LAS material with only a minor to moderate fraction of crystalline phases. The production of LAS glass-ceramics or ceramics with specified properties using the precursor gels synthesized as in the present study will, of course, require properly adjusted heat-treatment protocols and, potentially, the addition of nucleating agents or other auxiliary compounds.[18–20]

ACKNOWLEDGMENTS

This study was supported by internal funds by Bundesanstalt für Materialforschung und -prüfung (BAM) within the TF programme (project 'AFChem'). The authors thank Thi Bao Hoa Dao (BAM) for assistance in synthesizing the gels and Nico Vogler (BAM) for carrying out the thermogravimetric analyses.

Open access funding enabled and organized by Projekt DEAL.

CONFLICT OF INTEREST

The authors declare that they have no competing interest.

ORCID

Sebastian Simon https://orcid.org/0000-0002-2455-7239
Marko Bertmer https://orcid.org/0000-0002-3208-7927
Gregor J. G. Gluth https://orcid.org/0000-0002-8951-7393

REFERENCES

1. Scheidler H, Rodek E. Li_2O–Al_2O_3–SiO_2 glass-ceramics. Ceram Bull. 2004;68:1926–30.
2. Pannhorst W. Recent developments for commercial applications of low expansion glass ceramics. Glass Technol. 2004;45(2):51–3.
3. Kuhn A, Wilkening M, Heitjans P. Mechanically induced decrease of the Li conductivity in an alumosilicate glass. Solid State Ionics. 2009;180:302–7.
4. Ross S, Welsch A-M, Behrens H. Lithium conductivity in glasses of the LiO_2–Al_2O_3–SiO_2 system. Phys Chem Chem Phys. 2015;17:465–74.
5. Zocca A, Gomes CM, Bernardo E, Müller R, Günster J, Colombo P. LAS glass–ceramic scaffolds by three-dimensional printing. J Eur Ceram Soc. 2013;33:1525–33.
6. Simon S, Gluth GJG. Unraveling the hardening mechanism during laser-induced slip casting of lithium aluminate-microsilica slurry. Open Ceram. 2021;5:100060.
7. Lin J, Wen Z, Xu X, Li N, Song S. Characterization and improvement of water compatibility of γ-$LiAlO_2$ ceramic breeders. Fusion Eng Des. 2010;85:1162–6.
8. Choi H-J, Lee J-J, Hyun S-H, Lim H-C. Phase and microstructural stability of electrolyte matrix materials for molten carbonate fuel cells. Fuel Cells. 2010;10:613–8.
9. Gao J, Shi S, Xiao R, Li H. Synthesis and ionic transport mechanisms of α-$LiAlO_2$. Solid State Ionics. 2016;286:122–34.

10. Wohlmuth D, Epp V, Bottke P, Hanzu I, Bitschnau B, Letofsky-Papst I, et al. Order *vs.* disorder—a huge increase in ionic conductivity of nanocrystalline $LiAlO_2$ embedded in an amorphous-like matrix of lithium aluminate. J Mater Chem A. 2014;2:20295–306.
11. Beall GH, Pinckney LR. Nanophase glass-ceramics. J Am Ceram Soc. 1999;82:5–16.
12. Guedes M, Ferro AC, Ferreira JMF. Nucleation and crystal growth in commercial LAS compositions. J Eur Ceram Soc. 2001;21:1187–94.
13. Fu Q, Wheaton BR, Geisinger KL, Credle AJ, Wang J. Crystallization, microstructure, and viscosity evolutions in lithium aluminosilicate glass-ceramics. Front Mater. 2016;3:49.
14. O'Connor SJ, MacKenzie KJD. Synthesis, characterisation and thermal behaviour of lithium aluminosilicate inorganic polymers. J Mater Sci. 2010;45:3707–13.
15. Nourbakhsh AA, MacKenzie KJD, Jamshidi A. A novel method for the formation of lithium aluminosilicate and lithium aluminosilicate-alumina matrix composites by silicothermal reaction of Li-geopolymers. Mol Cryst Liq Cryst. 2013;577:116–26.
16. Colomban P. Chemical preparation routes and lowering the sintering temperature of ceramics. Ceramics. 2020;3:312–39.
17. Yang J-S, Sakka S, Yoko T, Kozuka H. Preparation of lithium aluminosilicate glass–ceramic monolith from metal–alkoxide solution. Part I. Preparation and properties of precursor gel monoliths. J Mater Sci. 1990;25:1773–8.
18. Yang J-S, Sakka S, Yoko T, Kozuka H. Preparation of lithium aluminosilicate glass-ceramic monolith from metal alkoxide solution. Part II. Conversion of gel to glass-ceramic monoliths and their properties. J Mater Sci. 1991;26:1827–33.
19. Lin MH, Wang MC. Crystallization behaviour of β-spodumene in the calcination of LiO_2–Al_2O_3–SiO_2–ZrO_2 gels. J Mater Sci. 1995;30:2716–21.
20. Bruneton E, Bigarré J, Michel D, Colomban P. Heterogeneity, nucleation, shrinkage and bloating in sol–gel glass ceramics (the case of lithium aluminosilicate compositions). J Mater Sci. 1997;32:3541–8.
21. Naskar MK, Chatterjee M. A novel process for the synthesis of lithium aluminum silicate powders from rice husk ash and other water-based precursor materials. Mater Lett. 2005;59:998–1003.
22. Chatterjee M, Naskar MK. Sol-gel synthesis of lithium aluminum silicate powders: the effect of silica source. Ceram Int. 2006;32:623–32.
23. Xia L, Wen G, Song L, Wang X. Sol–gel synthesis and crystallization behaviour of β-spodumene. J Sol-Gel Sci Technol. 2009;52:134–9.
24. Jiménez-Becerril J, García-Sosa I. Synthesis of lithium aluminate by thermal decomposition of a lithium dawsonite-type precursor. J Ceram Process Res. 2011;12:52–6.
25. Kerns L, Weinberg MC, Myers S, Assink R. Al coordination in sol–gel and conventional calcium aluminate glasses. J Non-Cryst Solids. 1998;232–4:86–92.
26. Radulović A, Dondur V, Vulić P, Miladinović Z, Ćirić-Marjanović G, Dimitrijević R. Routes of synthesis of nepheline-type polymorphs: an influence of Na-LTA bulk composition on its thermal transformation. J Phys Chem Solids. 2013;74:1212–20.
27. Gülgün MA, Nguyen MH, Kriven WM. Polymerized organic–inorganic synthesis of mixed oxides. J Am Ceram Soc. 1999;82:556–60.
28. Walkley B, San Nicolas R, Sani M-A, Gehman JD, van Deventer JSJ, Provis JL. Synthesis of stoichiometrically controlled reactive aluminosilicate and calcium-aluminosilicate powders. Powder Technol. 2016;297:17–33.
29. Rebouças LB, Souza MT, Raupp-Pereira F, Novaes de Oliveira AP. Characterization of LiO_2-Al_2O_3-SiO_2 glass-ceramics produced from a Brazilian spodumene concentrate. Cerâmica. 2019;65:366–77.
30. Andersen MD, Jakobsen HJ, Skibsted J. Effects of T_2-relaxation in MAS NMR spectra of the satellite transitions for quadrupolar nuclei: a ^{27}Al MAS and single-crystal NMR study of alum $KAl(SO_4)_2{\cdot}12H_2O$. J Magn Reson. 2005;173:209–17.
31. Massiot D, Fayon F, Capron M, King I, Calve SL, Alonso B, et al. Modelling one- and two-dimensional solid-state NMR spectra. Magn Reson Chem. 2002;40:70–6.
32. Poeppelmeier KR, Hwu S-J. Synthesis of lithium dialuminate by salt imbibition. Inorg Chem. 1987;26:3297–302.
33. Renaudin G, Rapin J-P, Humbert B, François M. Thermal behaviour of the nitrated AFm phase $Ca_4Al_2(OH)_{12}(NO_3)_2 \cdot 4H_2O$ and structure determination of the intermediate hydrate $Ca_4Al_2(OH)_{12}(NO_3)_2 \cdot 2H_2O$. Cem Concr Res. 2000;30:307–14.
34. Drewien CA, Tallant DR, Eatough MO. Thermal stability and decomposition kinetics of $Li_2Al_4CO_3(OH)_{12}{\cdot}3H_2O$. J Mater Sci. 1996;31:4321–5.
35. d'Espinose de la Caillerie J-B, Fretigny C, Massiot D. MAS NMR spectra of quadrupolar nuclei in disordered solids: the Czjzek model. J Magn Reson. 2008;192:244–51.
36. Vyalikh A, Zesewitz K, Scheler U. Hydrogen bonds and local symmetry in the crystal structure of gibbsite. Magn Reson Chem. 2010;48:877–81.
37. Koenig JJ, Angood AC. Raman spectra of poly(ethylene glycols) in solution. J Polym Sci Part A-2. 1970;8:1787–96.
38. Gontran E, Juchaux M, Deroulers C, Kruglik S, Huang N, Badoual N et al. Assessment of the ability of poly(L-lysine)-poly(ethylene glycol) (PLL-PEG) hydrogels to support the growth of U87-MG and F98 glioma tumor cells. J Appl Polym Sci. 2018;135:46287.
39. Kloprogge JT, Frost RL. Raman microscopy study of basic aluminium nitrate. Spectrochim Acta Part A. 1999;55:163–9.
40. Ruan HD, Frost RL, Kloprogge JT. Comparison of Raman spectra in characterizing gibbsite, bayerite, diaspore and boehmite. J Raman Spectrosc. 2001;32:745–50.
41. Watling HR, Sipos PM, Byrne L, Hefter GT, May PM. Raman, IR, and ^{27}Al-MAS-NMR spectroscopic studies of sodium (hydroxy)aluminates. Appl Spectrosc. 1999;53:415–22.
42. Renaudin G, Segni R, Mentel D, Nedelec J-M, Leroux F, Taviot-Gueho C. A Raman study of the sulfated cement hydrates: ettringite and monosulfoaluminate. J Adv Concr Technol. 2007;5:299–312.
43. McMillan P. Structural studies of silicate glasses and melts—applications and limitations of Raman spectroscopy. Am Mineral. 1984;69:622–44
44. Kirkpatrick RJ, Yarger JL, McMillan P, Yu P, Cong X. Raman spectroscopy of C–S–H, tobermorite, and jennite. Adv Cem Based Mater. 1997;5:93–9.
45. Renaudin G, Russias J, Leroux F, Cau-dit-Coumes C, Frizon F. Structural characterization of C–S–H and C–A–S–H samples—part II: local environment investigated by spectroscopic analyses. J Solid State Chem. 2009;182:3320–9.

46. Nesbitt HW, Henderson GS, Bancroft GM, O'Shaughnessy C. Electron densities over Si and O atoms of tetrahedra and their impact on Raman stretching frequencies and Si-NBO force constants. Chem Geol. 2017;461:65–74.
47. Arnault L, Gerland M, Rivière A. Microstructural study of two LAS-type glass-ceramics and their parent glass. J Mater Sci. 2000;35:2331–45.
48. Li C-T. Transformation mechanism between high-quartz and keatite phases of $LiAlSi_2O_6$ composition. Acta Crystallogr B. 1971;27:1132–40.
49. French BM, Jezek PA, Appleman DE. Virgilite: a new lithium aluminium silicate mineral from the Macusani glass, Peru. Am Mineral. 1978;63:461–5.
50. Isobe T, Watanabe T, d'Espinose de la Caillerie JB, Legrand AP, Massiot D. Solid-state ^{1}H and ^{27}Al NMR studies of amorphous aluminium hydroxides. J Colloid Interface Sci. 2003;261:320–4.
51. Serna CJ, Rendon JL, Iglesias JE. Crystal-chemical study of layered $[Al_2Li(OH)_6]^+X^-\bullet nH_2O$. Clays Clay Miner. 1982;30:180–4.
52. Frenkel M, Glasner A, Sarig S. Crystal modification of freshly precipitated aluminum hydroxide by lithium ion intercalation. J Phys Chem. 1980;84:507–10.

SUPPORTING INFORMATION

Additional supporting information can be found online in the Supporting Information section at the end of this article.

How to cite this article: Simon S, Bertmer M, Gluth GJG. Sol–gel synthesis and characterization of lithium aluminate (L–A–H) and lithium aluminosilicate (L–A–S–H) gels. Int J Appl Ceram Technol. 2022;19:3179–3190.
https://doi.org/10.1111/ijac.14187